EUROPEAN ORGANIZATION FOR NUCLEAR RESEARCH

CERN–ECP/95–1
January 1995

ANALOG LIGHTWAVE LINKS FOR DETECTOR FRONT-ENDS AT THE LHC

A. Baird[1], J. Dowell[2], P. Duthie[3], K. Gill[4], M. Glick[5], N.P. Green[3], G. Hall[4], R. Halsall[1], G. Jarlskog[6], L. Kennedy[3], I. Kenyon[2], A.J. Moseley[3], S. Quinton[1], D. Robbins[3], G. Stefanini[7], D.S. Streames-Smith[3], N.W. Try[3], F. Vasey[7] and K. Webster[2]

Abstract

Lightwave links are being developed for volume application in the transfer of analog signals from the tracking detector front-ends to their readout electronics. The links are based on electro-optic intensity modulators mounted on detectors and connected by optical fibres to remotely located transceivers (lasers and photoreceivers). The modulators are III-V semiconductor reflective devices based on multi-quantum well structures. The transceivers will be integrated devices of a novel design. Modulator prototypes have been fabricated and tested. Neutron and γ-ray irradiation studies have been performed on modulators and fibres. The main results achieved so far are reported and key system issues are reviewed. This work is part of the CERN DRDC project RD23.

Presented at the IEEE 1994 Nuclear Science Symposium
Norfolk, VA, October 30–November 5, 1994

---

[1] Rutherford Appleton Laboratory, Didcot (UK)
[2] School of Physics and Space Research, Univ. of Birmingham (UK).
[3] GEC-Marconi (Defence Systems – Materials Technology) (UK).
[4] Imperial College, London (UK).
[5] Institute of Micro- and Opto-electronics, EPFL, Lausanne (Switzerland).
[6] University of Lund (Sweden).
[7] CERN, Geneva (Switzerland).

1 INTRODUCTION

Several front-end electronics architectures are presently being investigated for the experiments at the CERN Large Hadron Collider (LHC): binary (discriminators), digital (analog pipelines followed by FADCs) and fully analog (pipelines only). Front-end data will be multiplexed and transferred to the readout stations, at a distance of ≈ 100 m, via optical links; copper links are ruled out due to bandwidth requirements and detector constraints.

The scheme based on analog pipelines and analog signal transfer offers significant advantages in signal-to-noise ratio and allows the complexity and power dissipation of the front-end electronics to be reduced [1]. It is presently planned to multiplex (at ≈ 40 MHz rate) the pipeline sampled voltages of 128 detector channels into one link; thus the readout of a tracker with ≈ 10 M channels will require ≈ 100 k analog optical links.

In the case of digital readout the degree of multiplexing is likely to be no larger than ≈ 1 k, and the corresponding number of optical links will still be considerable.

The front-end link components will be subject to severe requirements, particularly on radiation hardness (dose D ≈ 10 Mrad and fluence Φ ($\langle E_n \rangle \approx 1$ MeV) ≈ 10^{14}–10^{15} n/cm^2 over ≈ 10 years) and power dissipation (a few mW per optical channel). It is doubtful that these requirements can be satisfied by LEDs or laser diodes. The CERN RD23 project [2], started in 1992, is aimed at developing optical links based on external modulation of laser beams using electro-optic intensity modulators. These devices operate with power dissipation below 1 mW and are available in a technology which is inherently rad-hard. The RD23 project is supported by a CERN collaboration in partnership with industry (GEC-Marconi Defence Systems Ltd.). In this paper we report the main results achieved so far and review the key system issues.

2 ANALOG OPTICAL LINK CONFIGURATION

The analog readout architecture is currently based on reflective optical links as shown in Fig. 1 below.

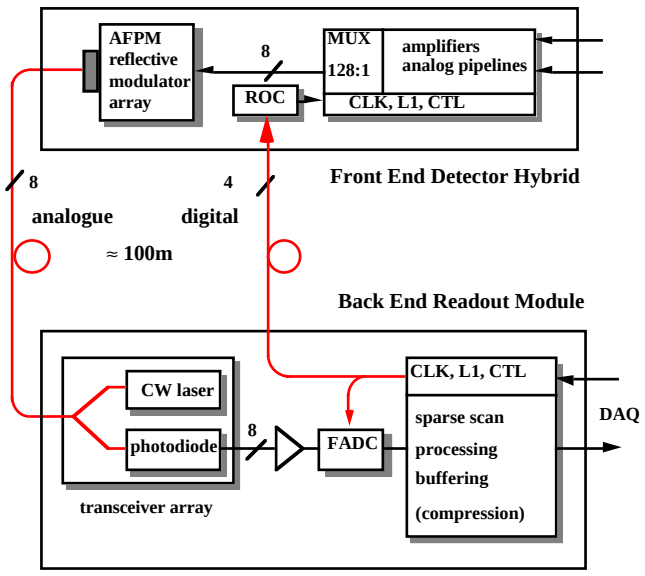

Fig. 1 Functional blocks of optical readout architecture.

The modulators, on the front-end detector hybrids, are coupled by fibres to the transceivers (lasers, fibre couplers and photoreceivers) located on the readout modules at the back end. The modulators reflect back a fraction of the continuous-wave (CW) incoming laser

beam, as determined by the applied input voltages (pipeline samples). In the transceiver, the reflected optical power is directed through the coupler onto the photoreceiver and converted back to an electrical signal.

Modulator and transceiver arrays are developed as integrated devices. It should be noted that these links are equally suitable for analog and digital transmission.

Timing and trigger signals are transferred to the front end via digital optical links. The constraints on these links are different from those used for readout, but certain components may be common to both.

3 REFLECTIVE MODULATORS

The modulators are asymmetric Fabry–Perot devices (AFPM) based on the electro-absorption properties of InGaAs/InP multi-quantum-well (MQW) structures on an InP substrate [3]. The operating wavelength is in the 1.55 μm window. This technology offers considerable advantages over the Mach–Zehnder interferometric modulators in lithium niobate ($Ti:LiNbO_3$) previously investigated [4, 5]. The AFPM are reflective devices and are polarization insensitive, thus each link requires a single input/output fibre of standard type. The vertical structure of these modulators is well suited for fabricating compact arrays at affordable cost and direct coupling to optical fibres. The intrinsic bandwidth of the AFPM extends from DC to ≈ 1 GHz, well beyond the needs of the present application.

The characteristics of the AFPM modulators have been investigated on four-channel arrays fabricated by GEC-Marconi Materials Technology (GMMT). The active MQW structures are 30 μm in diameter. The devices are pigtailed with SM fibre ribbons of 250 μm pitch. Several four-channel arrays have been fabricated. In the first prototypes the fibres were optically coupled to the modulator active region through the transparent InP substrate using relay microlenses. We have recently developed a novel compact assembly with butt-coupled fibres; this is described in Section 4. The ribbon fibre pigtail terminates in an MT ferrule within an MPO connector. The flat polished MT ferrules initially used are being replaced by the new angle-polished ferrules, which feature a higher return loss (> 50 dB). This results in a substantial reduction in the interferometric noise in the link, without the need for index matching gel. The typical transfer function of an AFPM is shown here in Fig. 2.

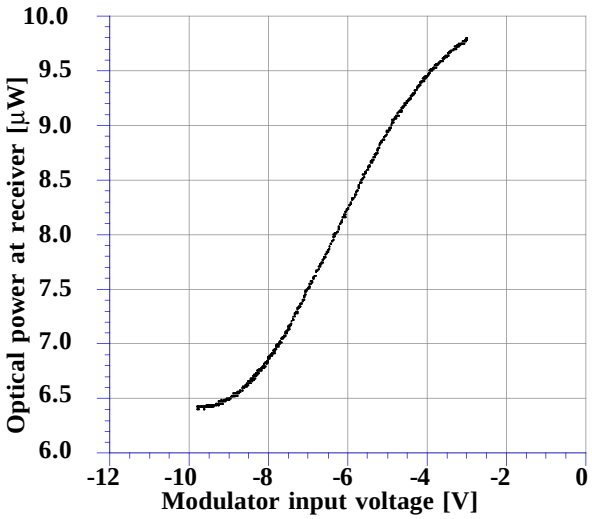

Fig. 2 AFPM transfer function.

The laser power launched in the modulator pigtail is ≈ 65 μW @ 1538 nm. The central region of the transfer function shows linear response (Fig. 3), with non-linearities contained within ≈ 2% of full scale for input signals in the range of ±1.5 V relative to the half-point bias (V_b ≈ –7 V). The full linear range corresponds to a reflectance changeδR ≈ 10%.

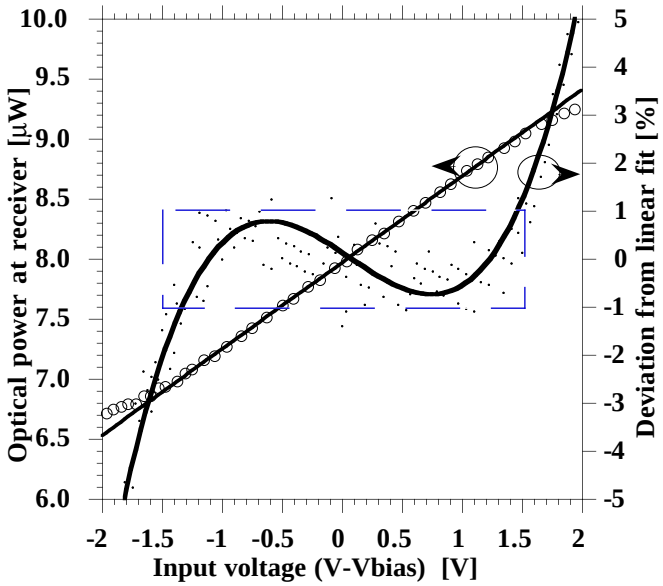

Fig. 3 AFPM linearity response.

The modulation characteristics of 14 working channels out of four packaged arrays are shown in Fig. 4. Two of these arrays, #4 and #5, were pigtailed with conventional flat polished MT ferrules. The other two, #7 and #8, were improved devices equipped with angle polished MTs. Measurements were taken with an input sine wave of amplitude δV = 1 Vpp (corresponding to ≈ 35% of the available dynamic range) and a CW laser power P_i ≈ 75 μW launched in the fibre. The differences in response can be accounted for by assembly tolerances.

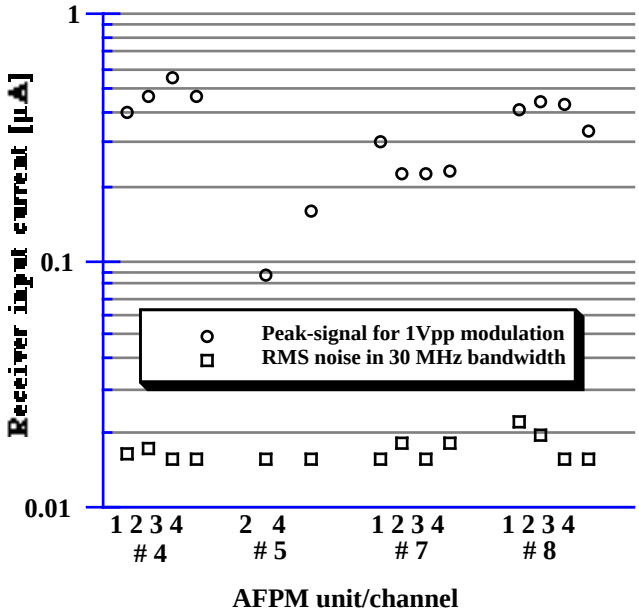

Fig. 4 Comparison of channels (micro-lens coupled devices).

4 AFPM WITH BUTT-COUPLED FIBRES

We have recently developed a novel assembly where the fibres are butt-coupled to the modulator active areas through the InP substrate, which is thinned down to ≈ 100 μm for this purpose. The assembly technique is based on a precision drilled substrate which determines the position and the orientation of the fibre ends with great accuracy. The semiconductor chip is aligned and bonded to the spacer using the solder-bump technique. A thin (≈ few μm) layer of optical glue assures the optical contact between the fibres and the semiconductor chip. The packaged array (Fig. 5) has a footprint of ≈ 10 × 10 mm and a height of ≈ 6 mm.

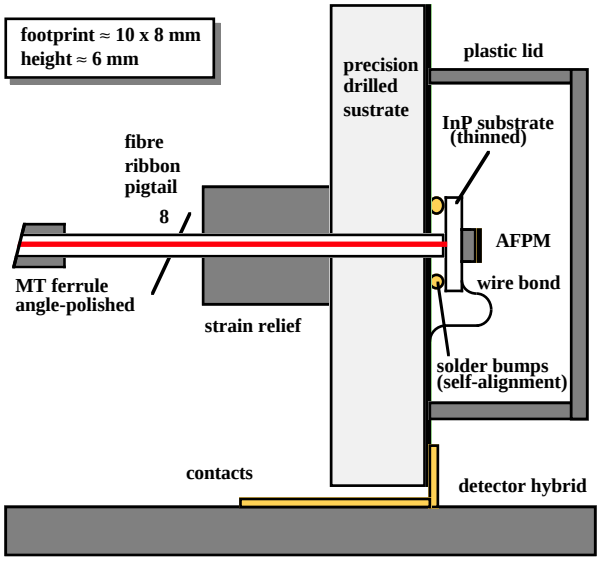

Fig. 5 Schematic of butt-coupled AFPM.

The prototypes are provided with flexible leads for simplicity of fabrication. Production devices will have solder pads or will be made as plug-in units to ease detector testing and mounting. The fibre ribbon pigtail has a length of several metres with a multi-way connector at the end, to provide a convenient breakout immediately outside the tracking detector region for installation in the experiment.

The butt-coupled AFPMs include an improved design of the Fabry–Perot cavity. On-wafer tests have confirmed that the tuning of the FP cavity resonance and the movement of the excitonic edge have fully met the design objectives. Two trial devices have recently been assembled and made available for evaluation. The optical insertion loss in the butt-coupled devices is equivalent to that of the microlensed devices, but is achieved in a compact package that is compatible with detector requirements. Other advantages of the new assembly are the much lower sensitivity to temperature changes and considerably reduced interferometric noise. Measurements are under way at the time of writing.

5 LINK PERFORMANCE

The overall link performance is determined by the contributions of the individual components, including fibre patchcords and optical connectors. The results reported here were obtained with a ≈ 100 m long fibre ribbon and a transceiver assembled with discrete fused fibre couplers. The equivalent input noise of the photoreceiver transimpedance amplifier was $I_n \approx$ 2.5 pA/√Hz and the measurement bandwidth extended from DC to ≈ 30 MHz.

5.1 Signal-to-noise ratio

A key feature of the analog link is the peak signal- to rms-noise ratio (S/N); this is determined under the constraint that nonlinearities should be contained within ≈ 2%. We have measured the S/N ratio with two types of laser diodes:

- A Fabry–Perot multimode laser, which is not very sensitive to back reflections and therefore allows a robust operation of the link. However, the relatively high laser noise (RIN ≈ –135 dB/Hz) sets a limit on the S/N ratio.
- A distributed feedback (DFB) laser, which features very low RIN (< –150 dB/Hz) but is very sensitive to back reflections so that intensity noise may be generated, even when angle-polished ferrules are used. To avoid this, an optical isolator is usually required, together with high-frequency (≈ 200 MHz) laser line dithering by RF modulation.

The modulator under test was unit #8 (microlensed device) fitted with an angle-polished MT ferrule.

The maximum S/N has been measured with a laser power of $P_I \approx 0.20$ mW launched into the modulator pigtail at the full-scale linear range modulation input of $\delta V = 3$ Vpp. We have obtained S/N ≈ 90 with the FP laser diode, and S/N ≈ 130 (typ.) in the case of the DFB laser diode, when the interferometric noise is reduced to a minimum. The results are shown in Fig. 6 below.

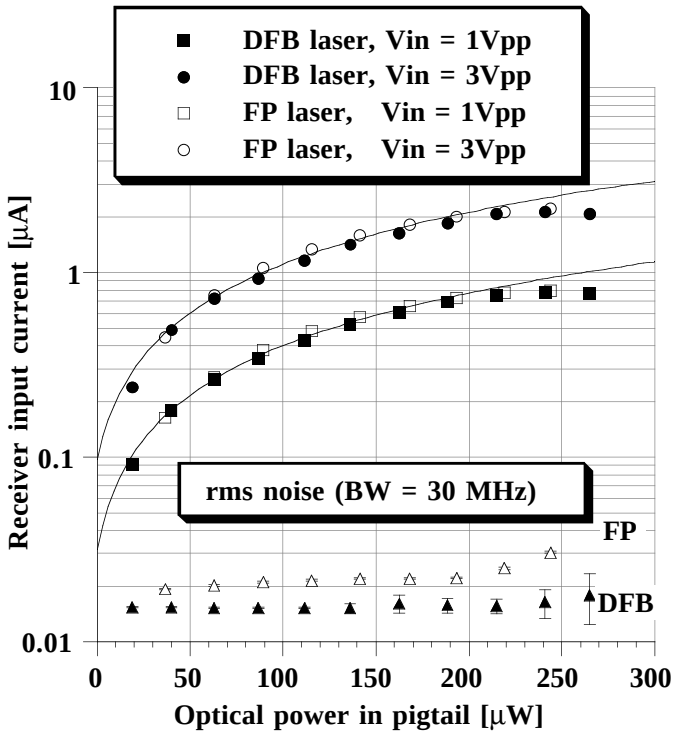

Fig. 6 Peak signal- to rms-noise ratio in the microlens coupled AFPM.

The S/N ratio should increase with laser input power up to a limiting value (S/N > 200) determined by the laser RIN. We find, however, that when the laser power is increased above ≈ 0.2 mW, the noise level also increases above the level expected from shot noise and RIN contributions, and it appears that S/N ≈ 150 is the best result that can be achieved at present. The effect is attributed to additional laser or interferometric noise or both resulting from increasing the optical power. Tests are under way to clarify this point.

Several improvements are envisaged to increase the S/N ratio if required. A reduction in the noise floor at low optical power will be obtained by using a transimpedance amplifier with lower input noise.

The maximum reflectivity change can be increased by optimizing the wafer growth and processing. It is expected that $\Delta R \approx 0.25$ to 0.3 can be achieved with good yield. This will increase the S/N ratio by $\approx 30\%$ relative to the best results obtained so far.

A further enhancement might be achieved by stacking two MQW regions; the stacked MQWs would be driven electrically in parallel, but the light would pass through both, so that the overall modulation efficiency could be increased.

5.2 Lab and beam tests with front-end electronics

The overall performance of the link was evaluated by comparing its response to a copper link (coaxial cable). In the lab, the input signal was a rectangular pulse of fixed amplitude. The output signals were measured with a digital scope (eight-bit resolution) and the data were collected and analysed using a LabVIEW-based DAQ. The two waveforms were normalized and the relative delay was determined by cross-correlation. Samples corresponding to the same region of the waveforms were compared and the error signal was evaluated. We found an approximately Gaussian distribution of the measured differences, with a deviation, $\sigma \approx \sigma_n$, where σ_n is the overall receiver noise contribution.

The performance of the optical link has also been evaluated in beam tests with the RD20 front-end chip APV3 [6] mounted on Si microstrip detectors (Fig. 7). The APV3 chip contains 32 channels and includes analog pipelines and APSP processors. The sampled voltages from the 32 channel pipelines were multiplexed in groups of eight into four optical links, using an external analog multiplexer running at ≈ 10 MHz. The peak signal amplitude was adjusted to either 0.4 or 0.8 V for an ~2 MIP energy loss, corresponding to a unipolar or bipolar operation of the modulator. The remaining part of the available link linear range (up to 3 V) was reserved to allow for the different and varying pedestal levels generated by the APV3 chip.

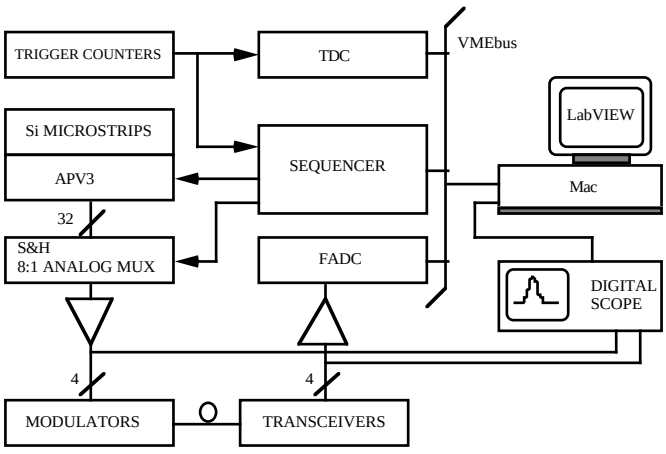

Fig. 7 Schematic of beam test setup.

The link was operated continuously for 36 hours with no degradation of the signal or noise characteristics. The only minor adjustments needed were due to the effects of temperature fluctuations in the beam area (a few degrees ˚C) on the micro-lens coupled assembly. Figure 8 shows the distribution (over 160 events) of the deviation of the signals measured simultaneously with both links.

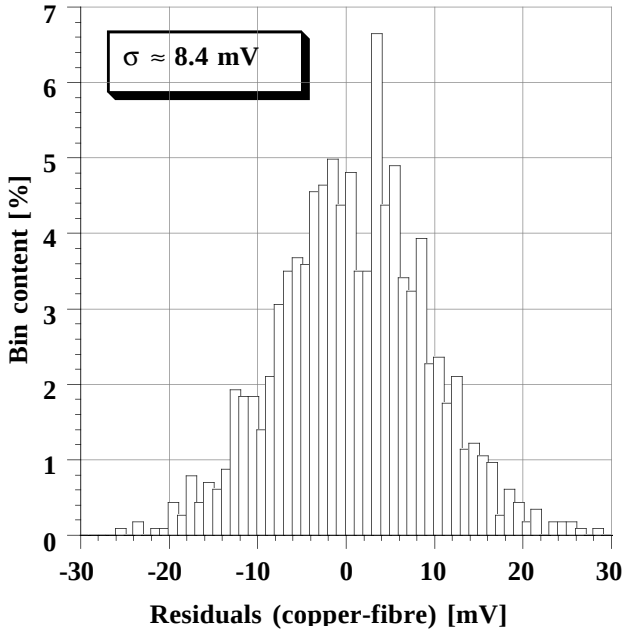

Fig. 8 Comparison of optical and copper links.

The receiver output signal amplitude corresponding to a mean 2 MIP energy loss was V_S ≈ 170 mV (laser power ≈ 200 μW in the fibre, signal amplitude ≈ 0.8 V at the modulator input). The standard deviation of the difference signal was σ ≈ 8.4 mV (rms) as shown. The increase in noise (σ ≈ 1.5 σ_n) was mainly due to residual non-linearities of the modulator. In practice, the results obtained with the two links were identical.

In the case of a 4 MIP full-scale energy loss, using the full linear input range (≈ 3 Vpp), we obtain σ_n ≈ 850 electrons (rms); this result is acceptable but needs to be improved for future applications.

6 EFFECTS OF MAGNETIC FIELDS AND TEMPERATURE CHANGES

Several MQW samples of varying well width (5 nm to 11.5 nm) were tested in fields up to 8 T. The transmission spectra were measured in fields oriented along the growth axis of the wells (largest effect) and at different angles. From these measurements, the shift in energy (wavelength) of the exciton peak and the change in peak absorption coefficient can be obtained.

The exciton peak shift is given by $\Delta E = c_1(w)\, B^2 + c_2(w)\, B^4$ where w is the well width. The parameters from the fit to the measured data were included in the device model, from which the induced reflectivity change δR was derived. It was found that when the field is parallel to the growth axis of the wells, the induced δR corresponding to the largest field expected in LHC detectors (≈ 4 T) is relatively small (δR < 2% with bias voltage V_b ≈ –7 to –10 V) and varies only slightly with well width. The effect of fields normal to the growth axis is considerably smaller [7]. These results confirm the general theoretical considerations and prove that magnetic fields will not induce any significant degradation in the link performance. Direct measurements on pigtailed modulators will be performed on the new devices which have suitable non-magnetic cases.

The main effect of temperature fluctuations is to change the relative positions of the excitons and the cavity wavelengths. According to the device model, the modulator operating temperature range for best performance will cover approximately +15 to –5˚C around the

design value, which can be tuned to the detector requirements. Outside this range the performance will start to degrade but will still be adequate for monitoring purposes. We have not yet been able to confirm the model predictions on the microlensed devices where the thermal effects due to the assembly (glued elements) predominate. Measurements are under way on the new butt-coupled devices.

7 INTEGRATED TRANSCEIVERS

Each channel of the reflective link requires a transceiver (laser/coupler/photodiode). In the present demonstrators, where a single laser feeds all channels in a modulator array, fused splitters and couplers are used. Discrete fibre optic components are commercially available, and offer a satisfactory solution in systems with a small number of channels. The volume production of transceivers for LHC application requires more cost-effective solutions. A preliminary comparison of the main alternatives can be summarized as follows:

- Integrated optics on glass. Passive optics (splitters and couplers) are implemented in planar technology (optical waveguides on a planar glass substrate). Lasers and photodiodes are connected by fibres. This technology is well suited for volume production. However, inquiries with several vendors prove that this solution would be too expensive.
- Monolithic opto-electronic integrated circuits (OEIC) on silicon submounts (Fig. 9). This technology has been demonstrated on several components. A key issue in the reflective link is to reduce the optical loss in the coupling of the silica fibre interface to the InP substrate waveguide. This might be achieved using tapered low NA waveguides, but substantial development work would be required. The OEIC offers potentially the lowest production cost if a satisfactory yield can be achieved.
- Planar opto-hybrid (Fig. 9). Silica-on-silicon waveguides allow for high efficiency coupling to optical fibres aligned using V-grooves. Lasers and photodiodes are die components. This technology may not lead to the lowest volume production cost, but the development would be less expensive and could be accomplished more rapidly than in the case of an OEIC.

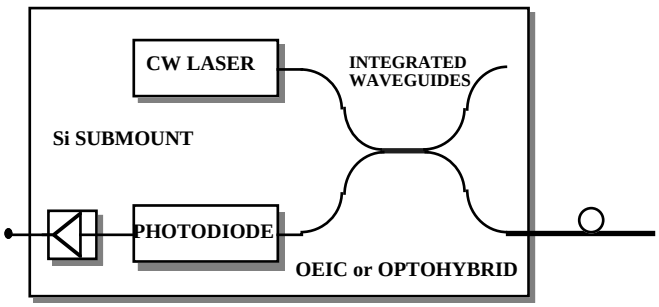

Fig. 9 Schematic of integrated transceiver.

A detailed investigation of the different technologies is under way. We expect that a planar opto-hybrid prototype could be delivered by around the end of 1995.

8 READOUT MODULE

We have developed a module that is a general link evaluation tool as well as the platform for a more complex system; the block diagram is shown below in Fig. 10.

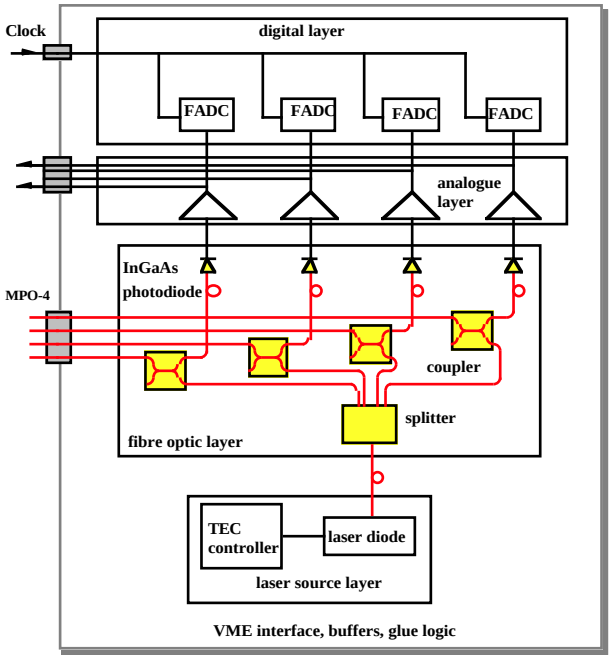

Fig. 10 Schematic of readout module prototype (four channels only shown).

The 6U VME module is designed to contain eight channels: splitter, couplers, receivers (InGaAs PIN photodiodes, amplifiers), eight-bit FADCs and FIFO buffers.

Low noise transimpedance amplifiers ($I_n \approx 2.5$ pA/$\sqrt{\text{Hz}}$), followed by a differential gain stage, assure an overall equivalent differential transresistance, $R_T \approx 600$ kOhm, with a bandwidth BW > 40 MHz. The amplifiers, mounted on daughterboards, deliver signals (< 2 Vpp amplitude for full linear modulation range) to the internal FADCs as well as to external digitizers through front-panel connectors.

The optical couplers — discrete fused fibre components — are assembled on a separate layer and fusion spliced to the photodiode pigtails. The laser diode feeds the modulator channels via an optical splitter.

Data are accessed through the VME interface and are also available on a parallel bus for fast transfer to auxiliary processing modules.

A prototype with four operational channels has been assembled and was used for the measurements reported in this document. The unit is designed to be fully modular for easy assembly and upgrading. Negotiations are currently under way with industrial firms with a view to engineering the module for small-scale production.

In the framework of the ATLAS and CMS experiments, we have undertaken a design study of a large-size single-width VME-type board with up to 64 optical channels [8]. Integrated transceivers are required to achieve this high packing density. The board will have full capabilities, including clock de-skewing and distribution, data reduction and addressing, and fast interface to the DAQ system. Prototypes with full signal processing functionality (without integrated transceivers) are expected by mid-1995.

9 SYSTEM ASPECTS

While the milestones in our project are mainly established by technical advances in modulators and integrated transceivers, we have become increasingly aware of system aspects

that are equally relevant for the feasibility and performance of the optical link. Some of the key issues being investigated are reviewed in this section.

Modulators are being developed as eight-channel arrays to make best use of the modularity of fibre ribbons and connectors that are industry standard. This modularity well fits a large part of the inner tracker detector elements and front-end electronics, with the devices mounted directly on the detector hybrids. In certain cases, it may be more cost-effective to mount the modulators on separate boards and fan-in the signals from two or more detector elements. The requirements on electrical line drivers and connectors are being investigated in collaboration with LHC experiments.

The fully analog readout of a 12 M-channel inner tracker may require up to ≈ 100 k fibres. The deployment of such a large number of fibres in the detector is a challenging task and requires enhanced packaging and connectivity. A possible scheme for the optical cabling is shown in Fig. 11.

We propose to use high-density matrix connectors (HDMX), developed and manufactured by Europtics (UK), which make use of the MT ferrule and provide up to 96 optical connections in approximately the area of a DIN 41612 connector shell. The matrix connectors contain MT ferrules which conform to CECC standards (the HDMX itself is being submitted for standardisation).

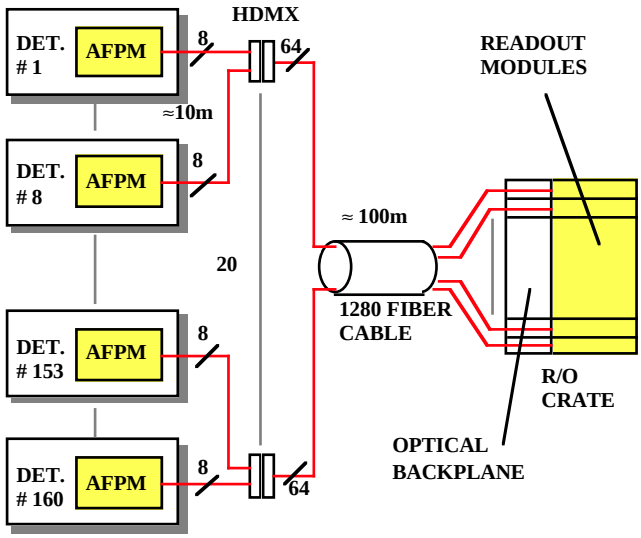

Fig. 11 Schematic of fibre cabling for the analog optical readout.

The optical cables will be installed pre-terminated with matrix connectors. After installation they will be plugged directly into dedicated optical connectors behind the readout crates. This approach offers both ease of installation — no fibre splicing is required — and good optical performance — the connectors are assembled in a quality controlled factory environment.

Digital optical links are required for distribution of the timing, trigger and control signals from the readout crate to the front-end electronics. In the scheme presently considered, the digital link would share a common ribbon with the analog readout fibres.

To minimize on cost and materials, integrating four photodiodes together with eight modulators in the same package, which would then be pigtailed with a 12-fibre ribbon, appears attractive. However, cross-talk (to be assessed) might prevent this integration, in which case

the 12-fibre ribbon would be bifurcated into an eight-way ribbon terminated in the modulator package and a four-way ribbon terminated in the photodiode package. The last approach allows the optimization of the two chips separately and the possible integration of the photodiode amplifier within the package. Similarly, at the readout end, the 12-fibre ribbon will be bifurcated and terminated on MT-8 and MT-4 ferrules, for analog and digital respectively. This technique would be cost-effective and allow redundancy.

The digital transmitters would be integrated low-power laser arrays, used in pulsed mode. The unavoidable differences in the lengths of the fibres carrying the timing signals will be compensated for by the de-skewing circuitry in the readout module.

10 IRRADIATION OF MODULATORS AND FIBRES

10.1 Modulators

Neutron irradiation of modulator structures has been performed at the ISIS facility at RAL with the fluence Φ ($\langle E_n \rangle$ = 1 MeV) $\approx 1.3 \times 10^{14}$ n/cm^2. The leakage current of some MQW devices increased from ≈ 1 nA to ≈ 100 nA — an increase attributed to surface effects. The spectral reflectance characteristics were measured before and after irradiation, and compared to the response of a reference device which was not irradiated. We could not detect any significant change in the spectral reflectance curve.

Modulator structures have recently been irradiated at the Imperial College ^{60}Co γ-ray source facility. The accumulated dose was D ≈ 20 Mrad, with a dose rate of dD/dt ≈ 205 krad per hour. Reflectance spectra were measured before and after irradiation, while the leakage current was monitored throughout the irradiation and recovery periods.

The spectral reflectance characteristics, as in the case of neutron irradiation, did not show any significant change.

Leakage current (at voltage bias ≈ –7 V) increased temporarily to a saturation level of ≈ 100 nA in some MQW devices, while it was not affected in others (Fig. 12).

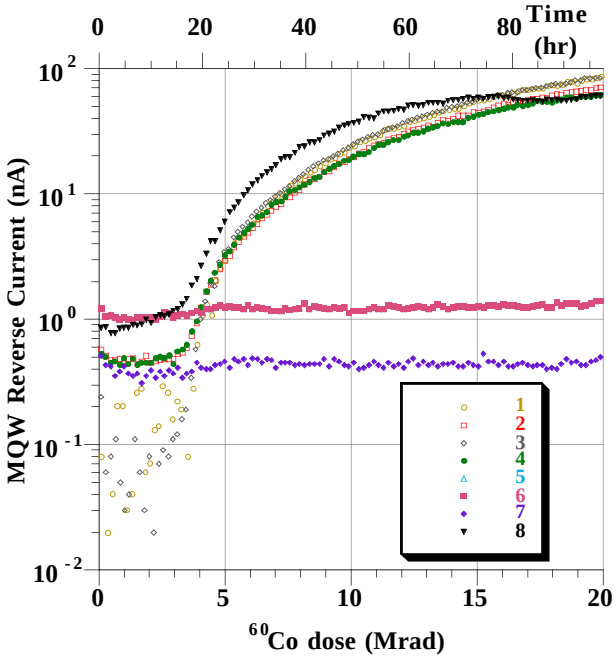

Fig. 12 AFPM samples — leakage current under gamma irradiation.

The increase in leakage current is attributed to the presence of a polyimide layer in the device structure; bulk InGaAs PIN diodes without this layer had previously been exposed to higher doses with no adverse effect.

Full recovery was observed in all cases, as shown in Fig. 13.

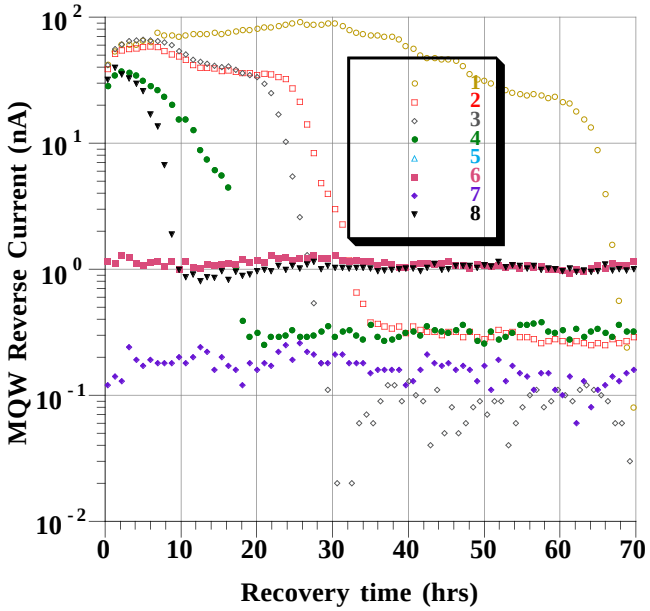

Fig. 13 AFPM samples — leakage current recovery after irradiation.

The results obtained so far indicate that the MQW structures are capable of withstanding the radiation levels at LHC without any significant degradation in optical and electrical performance. We plan to extend the irradiation measurements to the new butt-coupled devices, including the *in-situ* monitoring of the optical properties during exposure.

10.2 Fibres

The attenuation characteristics induced by neutron and γ-ray irradiation on optical fibres have been extensively investigated in several laboratories, particularly in view of the applications at nuclear power plants. Since the induced loss is considered to be related to the defects or 'colour centres' introduced by dopants such as Ge, pure-silica core fibres are expected to suffer the lowest loss. Theoretical models and experimental results can be found, for example, in Ref. [9].

We have measured the neutron and γ-ray irradiation damage on several types of fibres, mainly single-mode (SM) types. All the fibres tested are commercially available. This subsection contains a summary of the main results of the tests; a full report is to be submitted for publication [10].

Neutron irradiation runs were performed at the SARA facility in Grenoble. This facility delivers neutrons with a mean energy of 6.2 MeV from the Be(d,n)B reaction for irradiation at room and cryogenic temperature with fluence $\Phi \approx 5 \times 10^{14}$ n/cm^2. It may be recalled that $\Phi(\langle E_n \rangle = 6.2 \text{ MeV}) \approx 0.7\ \Phi(\langle E_n \rangle = 1 \text{ MeV})$ for the same non-ionising energy loss. The photon contamination is relatively low (≈ 22% of the total dose in CH_2 materials).

The samples irradiated at SARA included standard telecom SM Ge-doped and SM pure silica core, fluorine-doped (PSC/F2) fibres. Sample length was ≈ 70 m. The typical induced

attenuation (@ $\lambda = 1.3\ \mu m$ and $T \approx 20^{\circ}C$) for a neutron fluence of $\Phi \approx 10^{14}$ n/cm^2 is shown in the following table:

Table 1
Neutron irradiation at the SARA facility

SM Fibre type	$\Phi(\langle E_n \rangle \approx 6.2$ MeV) (n/cm^2)	Induced loss (dB/100 m)
PSC/F_2	1.2×10^{14}	0.25
Ge doped	4.0×10^{13}	1.0

These results were obtained at a fluence rate of $\approx 3.6 \times 10^{12}$ n/cm^2 per hour, while the corresponding rate at LHC, assuming six to twelve months' operation, would be $\approx 5 \times 10^{10}$ n/cm^2 per hour. In those conditions, taking into account the fibre recovery, the overall neutron-induced loss will be considerably smaller and it can be expected to have no significant effect on the link performance.

It is well known that dose rate effects of γ-ray irradiation can be very significant. The measurement of induced loss in a laboratory environment generally requires very high dose rates in order to reach a given accumulated dose D during irradiation runs that, for practical reasons, usually do not exceed a few days. Detailed models have been developed to extrapolate results where the same accumulated dose D is reached in a period of many years.

We have irradiated three types of single-mode fibres at the Imperial College ^{60}Co gamma source:

- pure silica core, fluorine doped cladding (PSC/F_2) — the same as in the neutron irradiation tests (types 1 and 2);
- match clad (MC), Ge-doped core for telecom applications (type 3).

Measurements were taken at 60-second intervals over six days during the irradiation, and for a further 32 hours after the irradiation in order to collect data on recovery. The accumulated dose and the dose rate were accurately measured for each fibre and are shown in Table 2 below:

Table 2
Total dose and dose rates

SM Fibre type	Dose D (Mrad)	Dose rate (krad/hr)
PSC/F_2 (type 1)	36	268
PSC/F_2 (type 2)	24	175
Ge doped	29	211

The time profile of the induced loss and recovery is shown in Fig. 14 for the three fibres. The data were fitted using the kinetic model referred to in Ref. [9], which is based on a rate equation of the growth and recombination of the defects at the constant dose rate dD/dt.

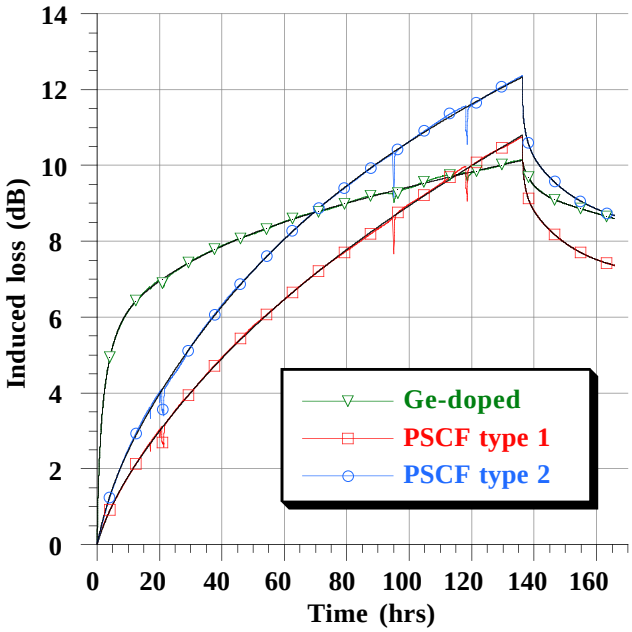

Fig. 14 Time profile of induced loss and recovery (fibre length ≈ 90 m).

According to this model, the induced loss is mainly determined by two terms: one depends only on the *total dose*, while the other is *dose-rate-dependent* and tends to saturation with increasing total dose. The second term is conveniently represented by the sum of two (or more) exponential components with different relaxation times. The dose rate dependent terms will give negligible contributions at the low dose rates found in the tracking region at the LHC.

To predict the induced loss at the LHC, we assume a machine operating cycle of six months of irradiation with dD/dt ≈ 500 rad/h followed by six months of recovery. The overall contribution of the rate-dependent terms will then be very low, and the corresponding residual induced loss will be fully recovered. The induced attenuation due to the linear term, in the worst case where there is no recovery during the six months of shutdown, is shown below in Table 3:

Table 3
Estimate of the γ-ray induced attenuation at the LHC

SM Fibre type	Induced loss (dB/100 m) (1 year)
PSC/F_2 (type 1)	0.3
PSC/F_2 (type 2)	0.6
Ge doped	0.2

In our scheme, the use of rad-hard fibre is limited to the modulator pigtail most exposed to high radiation levels. We assume that in the worst case the length of the pigtail would be ≈ 10 m, leading to an overall induced attenuation of less than 0.6 dB after 10 years of LHC operation.

It is interesting to note that, in the case of very low dose rates, the induced loss in the MC fibre, a Ge-doped type, seems to be comparable and even smaller than in the PSC/F_2 fibres. However, this type of fibre would be very sensitive to increased background levels or even minor beam spill accidents (dose rate), and we expect that it would show poor performance under neutron irradiation.

These results show that the radiation induced loss in the most exposed section of fibres — the modulator pigtail in the central region of the detector — will be negligible through the lifetime of an LHC experiment when single-mode PSC/F_2 fibres are used in the 1.5 μm wavelength window. These fibres are commercially available from several vendors at a slightly higher cost than standard telecom SM Ge-doped fibres, which can be safely used in the outer layers and for cabling in the experimental hall.

11 CONCLUSION

Analog lightwave links are being developed, in collaboration with industry, for volume application in LHC detectors. The key components of the links are semiconductor electro-optic modulators, integrated transceivers and ribbons of single-mode optical fibres.

Arrays of reflective InGaAs/InP modulators with micro-lens coupling to fibres have been fabricated and tested together with discrete component transceivers. The overall performance achieved so far is adequate for tracking detectors at the LHC. A novel compact modulator assembly with butt-coupled fibres has been developed for low-cost volume production. Several technologies for fabricating integrated transceivers have been investigated. A prototype is currently under development.

Modulator samples have been irradiated with neutrons and γ-rays to levels exceeding LHC detector requirements; no significant changes in the optical properties have been observed. Commercially available optical fibres with suitable radiation hardness have been identified and tested.

A receiver module prototype has been developed and design is under way of a full, large-size, high-density readout module for the LHC experiments.

A system approach to the optical cabling of the experiments is proposed, based on the specification of pre-tested assemblies; the key technology is the MT ferrule.

The work described is part of the CERN DRDC project RD23.

REFERENCES

[1] G. Hall and G. Stefanini, CMS TN/94–137.

[2] Status Reports on the RD23 project: CERN/DRDC/93–35 and CERN/DRDC/94–38.

[3] C. Kirkby, M. Goodwin, A. Moseley et al., IEEE Proc. **139** (1992) 249.

[4] T. Young et al., Proc. 6th Europ. Conf. on Integrated Optics (1993) 10.

[5] Nucl. Instr. and Meth. **A344** (1994) 199.

[6] CERN/DRDC/93–30 Status Report on the RD20 project.

[7] M. Haben, Thesis, University of Birmingham (unpublished);
K. Webster, ibid.; also, internal RD23 report by R. Cingolani and M. Glick.

[8] R. Halsall, S. Quinton et al., Specification of the readout module for the CMS tracker (RAL).

[9] M. Kyoto et al., Journ. Lightwave Technology **10** (1992) 289.

[10] K. Gill, N.Try, F. Vasey, CMS Technical Note 95–005 (1995).